Available online at www.sciencedirect.com
SCIENCE DIRECT®
Journal of Solid State Chemistry 178 (2005) 2191–2196
JOURNAL OF SOLID STATE CHEMISTRY
www.elsevier.com/locate/jssc

# High-temperature DTA studies of $A_xMF_3$ compounds ($A$ = K, Rb, Cs; $M$ = V, Cr; and $x = 0-1.0$)

Yun-Kang Yeh, Yaw-Shun Hong[1], William O.J. Boo, Daniell L. Mattern*

*Department of Chemistry and Biochemistry, University of Mississippi, University, MS 38677, USA*

Received 17 February 2005; received in revised form 19 April 2005; accepted 26 April 2005
Available online 31 May 2005

**Abstract**

$A_xVF_3$ ($A$ = K, Rb, Cs; $x = 0-1.0$) and $A_xCrF_3$ compounds were sealed inside high-temperature DTA molybdenum sample cups using electron beam welding techniques. Melting temperatures of the $A_xVF_3$ compounds ranged from 1050 to 1400 °C; those of $A_xCrF_3$ from 850 to 1200 °C. Reconstructive transitions were observed for $A_xVF_3$ compounds between 650 and 950 °C, and for $A_xCrF_3$ compounds between 550 and 825 °C. A displacive transition was observed to occur in $VF_3$ at 490 °C. Order–disorder transitions were determined by X-ray diffraction techniques. In the $A_xVF_3$ compounds, electronic ordering and ordering of partially filled $A^+$ sites were observed to occur between 100 and 300 °C. Ordering phenomena in the $A_xCrF_3$ compounds (in addition to electronic ordering and ordering of partially filled $A^+$ sites) included Jahn–Teller cooperative ordering. These compounded transitions occurred between 300 and 500 °C.


*Keywords:* Reconstructive transitions; Order–disorder transitions; Displacive transitions; Jahn–Teller cooperative ordering; Vanadium fluorides; Chromium fluorides

## 1. Introduction

Fig. 1 displays the generic ternary diagram $AF$–$MF_2$–$MF_3$ (where $A$ = K, Rb, Cs, or Tl and $M$ = V, Cr, or Fe). The line connecting $MF_3$ and $AMF_3$ defines a region which contains stable compounds. These compounds adhere to the general formula $A_xM^{II}_xM^{III}_{1-x}F_3$ ($A_xMF_3$, where $x$ varies from 0 to 1.0). Included phases are designated $MF_3$, $\alpha$, $\beta$, $\delta$, and $\gamma$. These phases are sometimes described as perovskite-like, because all $M$–F–$M$ bond angles are close to 180°. Moreover, they are $MF_3$ network structures in which $A^+$ ions occupy cagelike sites. Fractional values of $x$ are allowed because they are not a covalent part of the network. The sizes and relative compositions of the $A^+$ ions are determining factors as to which structures are stable. The composition spread for each phase also varies slightly with the choices of $M$ and $A$.

The lower-valence fluorides of vanadium, $A_xVF_3$, and chromium, $A_xCrF_3$ (where $A$ = K, Rb, or Cs), were first reported elsewhere [1–6], but their X-ray structures at 25 °C, along with those of $Tl_xVF_3$, were studied intensively in this laboratory [7–12]. Most of these materials demonstrate small crystal distortions and/or modulated structures, which are the consequence of concomitant ordering or displacive transitions that set in above 25 °C when they are cooled from higher temperatures.

Megaw [13] stated: "Structures may be said to belong to the same family if there is a one–to-one correspondence between all their atoms, and between their interatomic bonds". Furthermore, the symmetries

*Corresponding author. Fax: +1 662 915 7300.
*E-mail address:* mattern@olemiss.edu (D.L. Mattern).
[1]Present address: Department of Applied Chemistry, Chung Cheng Institute of Technology, Ta-Hsi, Taoyuan 33509, Taiwan, ROC.

0022-4596/$ - see front matter © 2005 Elsevier Inc. All rights reserved.
doi:10.1016/j.jssc.2005.04.028

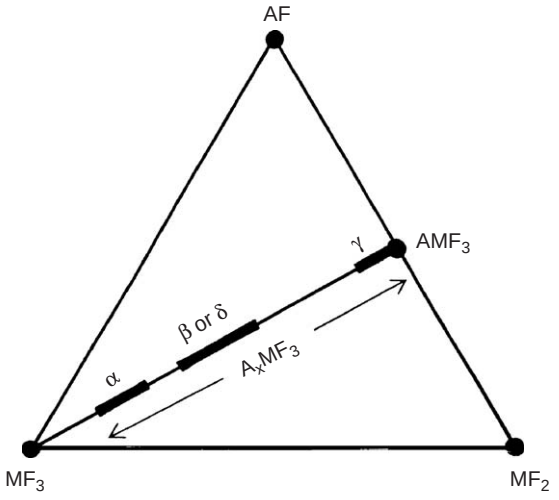


Fig. 1. The ternary diagram $A$F–$M$F$_2$–$M$F$_3$ (where $A$ = K, Rb, Cs, or Tl and $M$ = V, Cr, or Fe).

within a family of structures may differ. The simplest and most symmetrical member of a family is called the aristotype. Family members of lower symmetry are called hettotypes. Hettotype structures are sub-groups of the aristotype structure.

The aristotype structure of $MF_3$ is exemplified by the cubic form of $ReO_3$, space group $O_h^1$-$Pm\bar{3}m$ [14]. For the $\alpha$ phase it takes the hexagonal tungsten bronze structure of $K_xWO_3$, where $x = 0.18-0.32$ ($D_{6h}^3$-$P6_3/mcm$) [15]. The $\beta$ phase has two possible aristotype structures: tetragonal tungsten bronze, $K_xWO_3$ (where $x = 0.4-0.6$), space group ($D_{4h}^5$-$P4/mbm$) [16] and tetragonal tungsten bronze-like hexagonal $BaTa_2O_6$ ($D_{6h}^1$-$P6/mmm$) [17]. The $\delta$-phase aristotype is exemplified by the modified pyrochlore, $RbNiCrF_6$ ($O_h^7$-$Fd\bar{3}m$) [18], and for the $\gamma$ phase it is cubic perovskite, $CaTiO_3$ ($O_h^1$-$Pm\bar{3}m$) [14]. The structures of the $A_xVF_3$ and $A_xCrF_3$ compounds at 25 °C are mostly hettotypes of these aristotype structures.

The space groups of the hettotype structures $VF_3$ [19], $CrF_3$ [20], and $KCrF_3$ [21,22] were determined by single crystal X-ray diffraction methods. The hettotype structure for $K_xVF_3$ (tetragonal tungsten bronze) was deduced from magnetic susceptibility measurements [8]. The most probable space groups of all the other hettotype structures were obtained from Guinier–Hagg X-ray powder diffraction measurements made in this laboratory [23,24].

The structures of $VF_3$ [19] and $CrF_3$ [20] are rhombohedral ($D_{3d}^6$-$R\bar{3}c$) at 25 °C. Babel and Tressaud stated: "The high-temperature form of trifluorides in the $VF_3$ type appear to be of the $ReO_3$ type. For instance, $FeF_3$ is cubic above $T_{Tr} = 410$ °C" [25]. The melting temperatures of $VF_3$ and $CrF_3$ were reported to be 1406 and 1404 °C, respectively [26].

Three modulated structures were observed in the $\alpha$-phase regions of $A_xVF_3$ and $A_xCrF_3$. These correspond to $\frac{1}{2}$ filled $A^+$ sites where $x = 0.167$, $\frac{2}{3}$ filled $A^+$ sites for $x = 0.222$, and $\frac{3}{4}$ filled $A^+$ sites when $x = 0.250$. We designate these modulated structures $\alpha(167)$, $\alpha(222)$, and $\alpha(250)$, respectively. Each of the modulated structures belongs to a unique space group: $\alpha(167)$ belongs to $D_{2h}^{12}$-$Pnnm$, $\alpha(222)$ to $D_{2h}^{17}$-$Cmcm$, and $\alpha(250)$ to $D_{2h}^5$-$Pmma$. $\alpha(167)$ and $\alpha(222)$ are present in the $\alpha$ phase of $K_xVF_3$; all three modulated structures appear in the $\alpha$ phases of $Rb_xVF_3$, $Tl_xVF_3$, and $Rb_xCrF_3$; and $\alpha(222)$ and $\alpha(250)$ were found to be present in the $\alpha$ phase of $Cs_xCrF_3$. The $\alpha$ phase of $Cs_xVF_3$ displayed no superstructures but was distorted slightly to space group $D_{2h}^{17}$-$Cmcm$. The $\alpha$ phase of $K_xCrF_3$ also showed no evidence of superstructures, but was highly distorted, space group $D_{2h}^{13}$-$Pmmn$. No structural or thermal data have been reported for these materials at temperatures above 25 °C.

The $\beta$ phase of $K_xVF_3$ ($C_{4v}^8$-$P4_2bc$) is a hettotype of the tetragonal tungsten bronze structure [8]. The $\beta$ phase of $K_xCrF_3$ consists of three distinct structures at 25 °C [12]. The first, at the lowest range of $x$, is an aristotype structure corresponding to $BaTa_2O_6$ ($D_{6h}^1$-$P6/mmm$). The second is a hettotype of the $BaTa_2O_6$ structure ($D_{2h}^1$-$Cmmm$) existing in the middle range of $x$. For the highest range of $x$, there exists a third structure, which is a hettotype of tetragonal tungsten bronze, belonging to space group $C_{2v}^8$-$Pba2$. No high-temperature data has been reported for the $\beta$-phase compounds, except for the melting temperature of $K_{0.50}CrF_3$, which was reported to be 850 °C [6].

The $\delta$-phase compounds are hettotypes of the cubic $RbNiCrF_6$ structure. $Rb_xVF_3$ [23], $Rb_xCrF_3$ [24], and $Cs_xCrF_3$ [24] belong to space group $D_{2h}^7$-$Pmna$, but $Cs_xVF_3$ [23] belongs to $D_{2h}^{28}$-$Imma$. No data above 25 °C have been reported for any of the $\delta$-phase compounds.

$KVF_3$ has the aristotype structure of cubic perovskite ($O_h^1$-$Pm\bar{3}m$) [7]. The $KCrF_3$ structure ($D_{4h}^1$-$P4/mmm$) [6] is a hettotype of cubic perovskite. The tetragonal to cubic transition of $KCrF_3$ was reported to occur at 370 °C [27]. No other high-temperature data have been reported for the $\gamma$-phase compounds.

Table 1 summarizes the structures found in the $A_xVF_3$ and $A_xCrF_3$ systems. The phases are listed in the first column and their aristotype structures, including space groups, are given in the second column. The chemical formulas for each phase, and the range of $x$ over which the phase exists, are given in the third and fourth columns, respectively. Finally, the space groups of the structures (which are mostly hettotypes) are given in the last column. Note that the modulated structures $\alpha(167)$, $\alpha(222)$, and $\alpha(250)$ are found in the $\alpha$ phases of $K_xVF_3$, $Rb_xVF_3$, $Tl_xVF_3$, $Rb_xCrF_3$, and $Cs_xCrF_3$. These phases (which are not listed in Table 1) have composition spreads 0.19–0.27, 0.19–0.32, 0.19–0.30, 0.18–0.29 and

Table 1
Aristotype structures and their space groups, chemical formulas, range of $x$, and space groups of hettotype structures

| Phase | Aristotype structure and space group | Chemical formula | Range of $x$ | Space group of hettotype structure |
|---|---|---|---|---|
| $MF_3$ | $ReO_3$ | $VF_3$ | 0.0 | $D_{3d}^6$-$R\bar{3}c$ |
| | $O_h^1$-$Pm\bar{3}m$ | $CrF_3$ | 0.0 | $D_{3d}^6$-$R\bar{3}c$ |
| α | Hexagonal tungsten bronze | α(167) | 0.167 | $D_{2h}^{12}$-$Pnnm$ |
| | $D_{6h}^3$-$P6_3/mcm$ | α(222) | 0.222 | $D_{2h}^{17}$-$Cmcm$ |
| | | α(250) | 0.250 | $D_{2h}^5$-$Pmma$ |
| | | $Cs_xVF_3$ | 0.19–0.31 | $D_{2h}^{17}$-$Cmcm$ |
| | | $K_xCrF_3$ | 0.21–0.29 | $D_{2h}^{13}$-$Pmmn$ |
| β | Tetragonal tungsten bronze | $K_xVF_3$ | 0.45–0.56 | $C_{4v}^8$-$P4_2bc$ |
| | $D_{4h}^5$-$P4/mbm$ | $K_xCrF_3$ | 0.49–0.60 | $C_{2v}^8$-$Pba2$ |
| | Hexagonal $BaTa_2O_6$ | $K_xCrF_3$ | 0.43–0.50 | $D_{6h}^1$-$P6/mmm$ |
| | $D_{6h}^1$-$P6/mmm$ | $K_xCrF_3$ | 0.45–0.52 | $D_{2h}^1$-$Cmmm$ |
| δ | Modified pyrochlore $RbNiCrF_6$ | $Rb_xVF_3$ | 0.45–0.52 | $D_{2h}^7$-$Pmna$ |
| | $O_h^7$-$Fd\bar{3}m$ | $Cs_xVF_3$ | 0.45–0.52 | $D_{2h}^{28}$-$Imma$ |
| | | $Rb_xCrF_3$ | 0.50–0.58 | $D_{2h}^7$-$Pmna$ |
| | | $Cs_xCrF_3$ | 0.46–0.54 | $D_{2h}^7$-$Pmna$ |
| γ | Perovskite $CaTiO_3$ | $KVF_3$ | 1.0 | $O_h^1$-$Pm\bar{3}m$ |
| | $O_h^1$-$Pm\bar{3}m$ | $KCrF_3$ | 0.90–1.0 | $D_{4h}^1$-$P4/mmm$ |

0.19–0.26, respectively. The modulated structures exist as composition domains, and more than one exists in a sample of a given composition. $Rb_{0.225}VF_3$, for example, contains all three α-phase-modulated structures. Composition domains were also observed in the β-phase $K_xCrF_3$, which contains three distinct structures.

Our assumption is that, at elevated temperatures, the hettotype structures of the $A_xVF_3$ and $A_xCrF_3$ compounds will be transformed, via solid–solid phase transitions, to their respective aristotype structures. This has already been demonstrated with $KCrF_3$ and $FeF_3$. Furthermore, Babel and Tressaud [25] implied that $VF_3$ and $CrF_3$ will behave in a manner similar to $FeF_3$.

Fluorides are easily contaminated with trace amounts of oxygen at elevated temperatures. For this reason, very few high-temperature thermal or structural studies have been reported. In this study, high purity samples were vacuum encapsulated inside molybdenum DTA sample cups, thus eliminating the possibility of contamination by oxygen at high temperatures. High-temperature information about the $A_xVF_3$ and $A_xCrF_3$ compounds will lead to a better understanding of their dynamic structural properties. These data are also crucial prior to the preparation of single crystals.

The goals of this study were to determine the melting temperatures of these compounds, as well as the temperature regions over which their hettotype to aristotype (order–disorder) phase transitions occur, and to discover any unforseen solid–solid transitions that they might display.

## 2. Experimental

### 2.1. Materials

The compounds studied were previously characterized in this laboratory [7–12]. Every precaution was taken to ensure that the samples were oxygen free. Highly pure $VF_2$ [28], $VF_3$ [28], $CrF_2$ [29], and $CrF_3$ [24] were prepared in this laboratory as described elsewhere. Optical grade KF, RbF, and CsF obtained from Alfa Chemicals were dried in a vacuum oven at 550 °C and transferred directly to a desiccator, which in turn was transferred into an inert atmosphere glove box. Appropriate quantities of these materials were vacuum encapsulated inside molybdenum containers by electron-beam welding techniques and then fired at 800 °C for 28 days. All handling and transferring of materials was done inside an inert atmosphere glove box.

Products were analyzed optically by stereoscopic and polarized microscopy and further characterized by X-ray powder diffraction (25 °C) and magnetic measurements from 4.2 to 300 K [8–12]. Chemical analyses of K, Rb, Cs, V, and F in the $A_xVF_3$ compounds were in agreement with calculated values [7–10]. The $A_xCrF_3$ compounds were analyzed for K, Rb, Cs, and Cr; %F was taken by difference. %K, %Rb, %Cs, %Cr, and %F were in good agreement with calculated values [11,12].

### 2.2. Differential thermal analyses

Differential thermal analyses were run on a Perkin–Elmer DTA 1700 System, with a System 7/4

Thermal Analysis Controller. Thermocouples constructed of platinum and platinum/10% rhodium were used to monitor the temperatures of the sample and the reference material. Maximum furnace temperature of the system was 1500 °C.

DTA sample cups were machined from vapor-deposited solid molybdenum rods: 0.55 cm diameter × 0.85 cm long; wall thickness 0.05 cm. Thermocouple wells extended 0.35 cm below the bottom of the cup. The cups were fitted with lids which could be sealed vacuum tight using electron beam welding techniques. All molybdenum containers and DTA sample cups were baked out at 2000 °C in a Centorr Laboratory vacuum furnace equipped with tungsten mesh elements. Samples sealed inside the sample cups were ca. 100 mg. Weight checks were made after each step of the analysis to ensure that compositions of materials were unchanged from nominal values. Heating and cooling rates of 25 °C/min were used throughout all DTA measurements. All DTA heatings were replicated. The structures of all samples were characterized by Gunier–Hagg X-ray techniques both before and after DTA measurements.

### 2.3. X-ray measurements

High-temperature X-ray measurements were made on an Enraf–Nonius (Gunier–Simon) high-temperature X-ray camera. High-temperature X-ray measurements were of an exploratory nature. Samples were selected for each of three categories: (1) ordering of partially filled $A^+$ sites [$T1_{0.18}VF_3$, mostly $\alpha(167)$]; (2) electronic ordering [$Rb_{0.50}VF_3$]; and (3) Jahn–Teller cooperative ordering [$K_{0.575}CrF_3$] and [$Rb_{0.50}CrF_3$]. The fluoride samples were encapsulated inside dry quartz capillaries. X-ray measurements were made at 100° intervals. The exposure time for each temperature setting was 12 h.

## 3. Results

### 3.1. DTA

The DTA peaks associated with melting temperatures were well defined in every case. In contrast, many of the peaks associated with solid–solid transitions were small. The results of DTA measurements are summarized in

Table 2
High-temperature DTA results

| Compound | Melting point (°C) | Solid-state transition temps (°C) | X-ray structure of sample at 25 °C after DTA |
|---|---|---|---|
| $VF_3$ | 1395 | (490 s) | Sample lost |
| $CrF_3$ | 1188 | — | Sample lost |
| $K_{0.18}VF_3$ | 1257 | (775 s)(880 s) | Unchanged |
| $K_{0.225}VF_3$ | 1277 | (770 m)(863 s) | $\alpha(222)$ disappeared |
| $K_{0.50}VF_3$ | 1057 | (806, 1) | Unchanged |
| $KVF_3$ | 1130 | — | Unchanged |
| $K_{0.25}CrF_3$ | 1022 | (651 vs) | Sample lost |
| $K_{0.45}CrF_3$ | 895 | (569 vs)(753, 1) | $C_{2v}^8$-*Pba*2 |
| $K_{0.55}CrF_3$ | 881 | (565 vs)(757, 1) | $C_{2v}^8$-*Pba*2 |
| $K_{0.55}CrF_3$ | 870 | (565 vs)(758, 1) | $C_{2v}^8$-*Pba*2 (unchanged) |
| $KCrF_3$ | 863 | (378 s) | Unchanged |
| $Rb_{0.18}VF_3$ | 1311 | (780 s)(958 s) | Unchanged |
| $Rb_{0.20}VF_3$ | 1322 | (792 s)(966 s) | $\alpha(222)$ disappeared |
| $Rb_{0.225}VF_3$ | 1310 | (781 s)(941 s) | $\alpha(222)$ and $\alpha(250)$ disappeared |
| $Rb_{0.250}VF_3$ | 1316 | (646 s)(930 s) | $\alpha(222)$ and $\alpha(250)$ disappeared |
| $Rb_{0.275}VF_3$ | 1318 | (783 m)(934 m) | $\alpha(222)$ and $\alpha(250)$ disappeared |
| $Rb_{0.30}VF_3$ | 1279 | (778 s)(936 s) | Unchanged |
| $Rb_{0.50}VF_3$ | 1206 | (903 m) | Unchanged |
| $Rb_{0.18}CrF_3$ | 1103 | (807 m) | Unchanged |
| $Rb_{0.20}CrF_3$ | 1134 | (807 m) | $\alpha(222)$ disappeared |
| $Rb_{0.225}CrF_3$ | 1129 | (808 m) | $\alpha(222)$ and $\alpha(250)$ disappeared |
| $Rb_{0.250}CrF_3$ | 1110 | (805, 1) | $\alpha(222)$ and $\alpha(250)$ disappeared |
| $Rb_{0.275}CrF_3$ | 1106 | (800 m) | $\alpha(222)$ and $\alpha(250)$ disappeared |
| $Rb_{0.30}CrF_3$ | 1072 | (805 m) | Unchanged |
| $Rb_{0.50}CrF_3$ | 1018 | (710 m) | Unchanged |
| $Cs_{0.25}VF_3$ | 1327 | (811 vs) | Unchanged |
| $Cs_{0.45}VF_3$ | 1255 | (888 s) | Unchanged |
| $Cs_{0.50}VF_3$ | 1250 | (865 s) | Unchanged |
| $Cs_{0.25}CrF_3$ | 1115 | (825 m) | $\alpha(222)$ and $\alpha(250)$ disappeared |
| $Cs_{0.50}CrF_3$ | 1101 | (784 s) | Unchanged |

Table 2. The first column in the table lists the compounds that were run. The second column gives the melting temperature of each compound. The third column lists temperatures of solid–solid phase changes; the relative magnitudes of these peaks are reported as vs (very small), s (small), m (medium), and l (large). The last column in Table 2 gives X-ray results on samples at 25 °C, after DTA measurements were made on them.

### 3.2. High-temperature X-ray

The intensities of superlattice reflections of $Tl_{0.18}VF_3$ were relatively strong at 21 and 100 °C. At 200 °C these intensities were diminished by approximately half and at 300 °C they appeared to be completely absent. The remaining X-ray reflections were fitted to a hexagonal lattice of dimensions $a = 7.45$ Å, $c = 7.56$ Å. The modified pyrochlore compound $Rb_{0.50}VF_3$ was orthorhombic at 21 and 100 °C. By 200 °C it had changed to cubic, $a = 10.4$ Å. The corresponding modified pyrochlore compound $Rb_{0.50}CrF_3$ was orthorhombic at 21, 100, 200, 300, and 400 °C. Between 400 and 500 °C it changed to cubic, $a = 10.2$ Å. The tetragonal tungsten bronze-type compound $K_{0.575}CrF_3$ was orthorhombic at 21, 100, 200, and 300 °C. By 400 °C it had changed to tetragonal, $a = 13.1$ Å, $c = 3.94$ Å.

## 4. Discussion

The melting temperature determined for $VF_3$ (1395 °C) is in good agreement with the 1406 °C reported by Strum [26]. However, our value for $CrF_3$ (1188 °C) is approximately 200° lower than his value (1404 °C). The melting temperature of $K_{0.50}CrF_3$ (903 °C) differs slightly from that reported by Dumora et al. (850 °C) [6].

The small DTA peak of $VF_3$ at 490 °C compares closely to the (rhombohedral → cubic) transition reported for $FeF_3$ (410 °C) [25]. The $CrF_3$ sample, however, was a light fluffy powder (in contrast to $VF_3$, which was dense), which is probably the reason the (rhombohedral → cubic) transition of $CrF_3$ was not observed. The Jahn–Teller transition of $KCrF_3$ (376 °C) is in excellent agreement with the 370 °C reported by Cousseins et al. [27].

The approximate temperatures of four order–disorder transitions were identified by X-ray diffraction. (1) The (ordering of partially filled $A^+$ sites) transition of $Tl_{0.18}VF_3$, in which the α(167) superlattice X-ray reflections disappear, occurs slowly over the range 100–300 °C. (2) The (orthorhombic→cubic) transition of $Rb_{0.50}VF_3$, attributed to electronic ordering, occurs between 100 and 200 °C. (3) The (orthorhombic→cubic) transition of $Rb_{0.50}CrF_3$, associated with Jahn–Teller cooperative ordering, occurs between 400 and 500 °C; and (4) the (orthorhombic→tetragonal) transition of $K_{0.575}CrF_3$, also associated with Jahn–Teller ordering, occurs between 300 and 400 °C. These four transitions represent the three types of order–disorder phenomena which occur in the $A_xVF_3$ and $A_xCrF_3$ compounds above room temperature. We assume from this experimental evidence that all of the order–disorder transitions in these compounds most likely occur below 500 °C, and that the enthalpy changes associated with them are too small to be observed by DTA.

The solid–solid transitions listed in Table 2 obviously do not belong to order–disorder transitions, since they occur at temperatures which are too high and their enthalpies are too large. The fact that the DTA peaks were observed at all argues that they correspond to reconstructive transitions.

At high temperatures, the $AMF_3$ ($A = K$, Rb) compounds have the cubic perovskite structure. The high-temperature structures of the $MF_3$ compounds may also be described as cubic perovskite, but with vacant $A^+$ sites. The question is: does the cubic perovskite structure exist at high temperatures where $A^+$ sites are partially filled? If it does, there are two conditions which must be met. (1) There must be reconstructive transitions below the melting temperatures and (2) melting temperatures (including those of $MF_3$) on a plot of temperature versus $x$ must lie on a smooth curve.

We see from Table 2 that the first condition is met for every $A_xVF_3$ and $A_xCrF_3$ compound. Fig. 2 is a plot of melting temperatures versus $x$ (up to $x = 0.55$) of ($K_xVF_3$ and $K_xCrF_3$), ($Rb_xVF_3$ and $Rb_xCrF_3$), and ($Cs_xVF_3$ and $Cs_xCrF_3$). In each case (except $Cs_xCrF_3$) the melting temperatures lie approximately on a straight line. Since we know that $VF_3$ and $CrF_3$ have cubic perovskite-like structures, the $A_xMF_3$ compounds (with the possible exception of $Cs_xCrF_3$) must belong to perovskite phases in which $A^+$ sites are partially filled.

Figs. 2a–c reveal that the melting temperatures of the $A_xVF_3$ compounds are approximately 200 °C higher than their chromium analogs. We also note that the melting point of $CrF_3$ reported by Strum [26] must be in error.

The X-ray structures of several samples were different after the DTA measurements (see Table 2). The modulated structures α(222) and α(250) did not form again upon rapid cooling, but α(167) did so in every case. The samples $K_{0.45}CrF_3$ (hexagonal $BaTa_2O_6$ structure); $K_{0.50}CrF_3$ (hexagonal $BaTa_2O_6$ structure distorted to orthorhombic); and $K_{0.55}CrF_3$ (tetragonal tungsten bronze structure distorted to orthorhombic) all had the distorted tetragonal tungsten bronze structure after DTA. This is a curious result, as the French authors [6] reported growing a single crystal which had the hexagonal $BaTa_2O_6$ structure. This implies that the method of preparation and/or the thermal history of these materials play important roles as to what structures are formed.

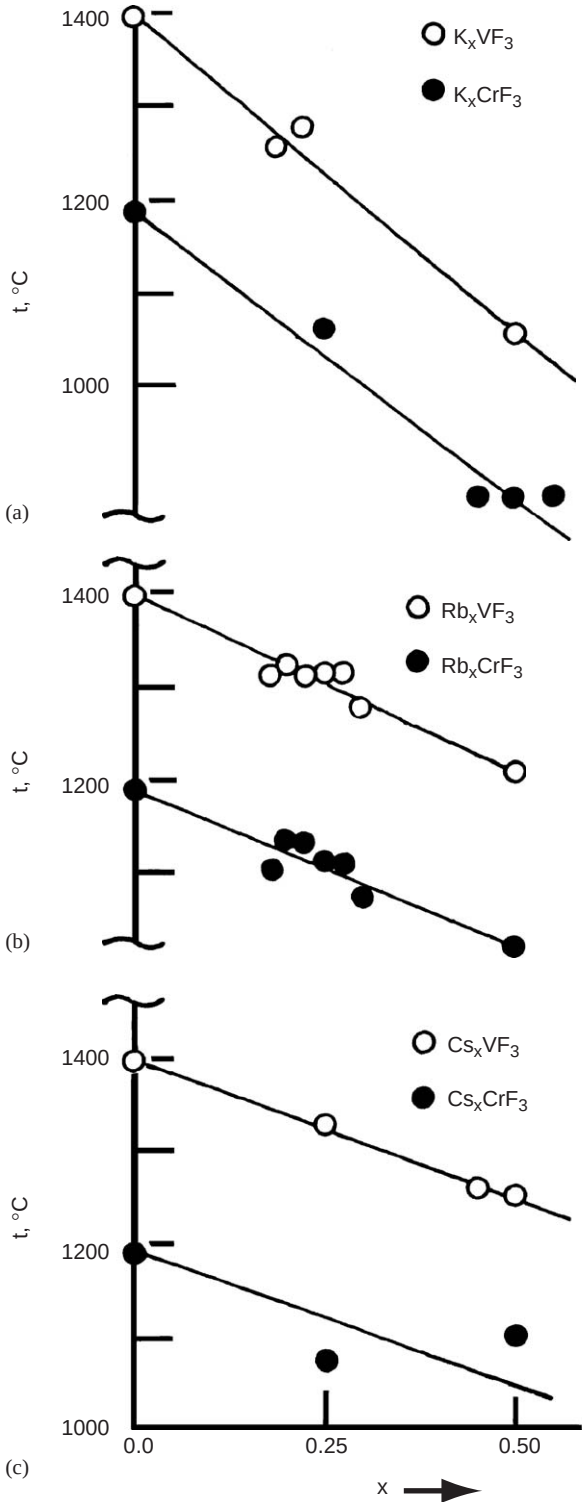


Fig. 2. Melting temperature versus $x$ of (a) $K_xVF_3$ and $K_xCrF_3$, (b) $Rb_xVF_3$ and $Rb_xCrF_3$, and (c) $Cs_xVF_3$ and $Cs_xCrF_3$.

## 5. Conclusions

The high-temperature behaviors of the $A_xVF_3$ and $A_xCrF_3$ compounds were not understood prior to this study. The original goals of this study were met: melting temperatures of the compounds were determined, the temperature regions over which order–disorder transitions and displacement transitions occur were identified, and unforseen solid–solid transitions were discovered. The melting temperatures of the $A_xVF_3$ compounds were approximately 200 °C higher than their $A_xCrF_3$ analogs. Order–disorder transitions, which include electronic ordering and ordering of partially filled $A^+$ sites in the $A_xVF_3$ compounds, occur between 100 and 300 °C. These same transitions, when accompanied by Jahn–Teller ordering, occur in the $A_xCrF_3$ compounds at slightly higher temperatures. At temperatures close to melting, all of the $A_xVF_3$ and $A_xCrF_3$ compounds appear to undergo reconstructive transitions to form cubic perovskite type phases.

## References

[1] M.W. Shafer, Mater. Res. Bull. 4 (1969) 905.
[2] C. Cros, R. Feurer, M. Pouchard, P. Hagenmuller, Rev. Chim. Miner. 11 (1974) 585.
[3] C. Cros, R. Feurer, J.C. Grenier, M. Pouchard, Mater. Res. Bull. 11 (1976) 117.
[4] C. Cros, M. Feurer, M. Pouchard, P. Hagenmuller, Mater. Res. Bull. 10 (1975) 383.
[5] D. Dumora, J. Ravez, P. Hagenmuller, J. Solid State Chem. 5 (1972) 35.
[6] D. Dumora, J. Ravez, P. Hagenmuller, Bull. Soc. Chim. Fr. 5 (1970) 1751.
[7] R.F. Williamson, W.O.J. Boo, Inorg. Chem. 16 (1977) 646.
[8] Y.S. Hong, R.F. Williamson, W.O.J. Boo, Inorg. Chem. 19 (1980) 2229.
[9] Y.S. Hong, R.F. Williamson, W.O.J. Boo, Inorg. Chem. 20 (1981) 403.
[10] Y.S. Hong, R.F. Williamson, W.O.J. Boo, Inorg. Chem. 21 (1982) 3898.
[11] Y.S. Hong, K.N. Baker, R.F. Williamson, W.O.J. Boo, Inorg. Chem. 23 (1984) 2787.
[12] Y.S. Hong, K.N. Baker, A.V. Shah, R.F. Williamson, W.O.J. Boo, Inorg. Chem. 29 (1990) 3037.
[13] H.D. Megaw, Crystal Structures: A Working Approach, Saunders, Philadelphia, 1973, p. 282.
[14] A.F. Wells, Structural Inorganic Chemistry, Oxford University Press, London, 1962, p. 495.
[15] A. Magneli, Acta Chem. Scand. 1 (1953) 315.
[16] A. Magneli, Ark. Kemi. 1 (1949) 213.
[17] G.K. Layden, Mater. Res. Bull. 3 (1968) 349.
[18] D. Babel, G. Pausewang, W. Viebahn, Z. Naturforsch. 22B (1967) 1219.
[19] K.H. Jack, V. Gutman, Acta Crystallogr. 4 (1951) 246.
[20] K. Knox, Acta Crystallogr. 13 (1960) 507.
[21] K. Knox, Acta Crystallogr. 14 (1961) 583.
[22] A.I. Edwards, R.D. Peacock, J. Chem. Soc. 4 (1959) 4126.
[23] Y.S. Hong, Ph.D. Dissertation, University of Mississippi, 1980, unpublished.
[24] K.N. Baker, Ph.D. Dissertation, University of Mississippi, 1986, unpublished.
[25] D. Babel, A. Tressaud, in: P. Hagenmuller (Ed.), Inorganic Solid Fluorides, Chemistry and Physics, Academic Press, Orlando, FL, 1985, p. 94.
[26] B.J. Strum, Inorg. Chem. 1 (1962) 665.
[27] J.C. Cousseins, A.C. Kozak, R. Acad. Sci. 263 (1966) 1533.
[28] J.W. Stout, W.O.J. Boo, J. Chem. Phys. 71 (1979) 1.
[29] W.O.J. Boo, J.W. Stout, J. Chem. Phys. 71 (1979) 9.